Available online at www.sciencedirect.com
ScienceDirect
Journal of Computational Physics 224 (2007) 40–58
JOURNAL OF COMPUTATIONAL PHYSICS
www.elsevier.com/locate/jcp

An extended pressure finite element space for two-phase incompressible flows with surface tension

Sven Groß *,[1], Arnold Reusken

Institut für Geometrie und Praktische Mathematik, RWTH Aachen, Templergraben 55, D-52056 Aachen, Germany

Received 19 September 2006; received in revised form 6 December 2006; accepted 20 December 2006
Available online 10 January 2007

Abstract

We consider a standard model for incompressible two-phase flows in which a localized force at the interface describes the effect of surface tension. If a level set (or VOF) method is applied then the interface, which is implicitly given by the zero level of the level set function, is in general not aligned with the triangulation that is used in the discretization of the flow problem. This non-alignment causes severe difficulties w.r.t. the discretization of the localized surface tension force and the discretization of the flow variables. In cases with large surface tension forces the pressure has a large jump across the interface. In standard finite element spaces, due to the non-alignment, the functions are continuous across the interface and thus not appropriate for the approximation of the discontinuous pressure. In many simulations these effects cause large oscillations of the velocity close to the interface, so-called spurious velocities. In this paper, for a simplified model problem, we give an analysis that explains why known (standard) methods for discretization of the localized force term and for discretization of the pressure variable often yield large spurious velocities. In the paper [S. Groß, A. Reusken, Finite element discretization error analysis of a surface tension force in two-phase incompressible flows, Preprint 262, IGPM, RWTH Aachen, SIAM J. Numer. Anal. (accepted for publication)], we introduce a new and accurate method for approximation of the surface tension force. In the present paper, we use the extended finite element space (XFEM), presented in [N. Moes, J. Dolbow, T. Belytschko, A finite element method for crack growth without remeshing, Int. J. Numer. Meth. Eng. 46 (1999) 131–150; T. Belytschko, N. Moes, S. Usui, C. Parimi, Arbitrary discontinuities in finite elements, Int. J. Numer. Meth. Eng. 50 (2001) 993–1013], for the discretization of the pressure. We show that the size of spurious velocities is reduced substantially, provided we use both the new treatment of the surface tension force and the extended pressure finite element space.

MSC: 65M60; 65N15; 65N30; 76D45; 76T99

Keywords: Pressure finite element space; Two-phase flow; Surface tension; Spurious velocities

* Corresponding author. Tel.: +49 241 8097068; fax: +49 241 8092349.
E-mail addresses: gross@igpm.rwth-aachen.de (S. Groß), reusken@igpm.rwth-aachen.de (A. Reusken).
[1] Supported by the German Research Foundation through SFB 540.

0021-9991/$ - see front matter © 2007 Elsevier Inc. All rights reserved.
doi:10.1016/j.jcp.2006.12.021

1. Introduction

Let $\Omega \subset \mathbb{R}^3$ be a convex polyhedral domain containing two different immiscible incompressible phases. The time dependent subdomains containing the two phases are denoted by $\Omega_1(t)$ and $\Omega_2(t)$ with $\bar{\Omega} = \bar{\Omega}_1 \cup \bar{\Omega}_2$ and $\Omega_1 \cap \Omega_2 = \emptyset$. We assume that Ω_1 and Ω_2 are connected and $\partial\Omega_1 \cap \partial\Omega = \emptyset$ (i.e., Ω_1 is completely contained in Ω). The interface is denoted by $\Gamma(t) = \bar{\Omega}_1(t) \cap \bar{\Omega}_2(t)$. The standard model for describing incompressible two-phase flows consists of the Navier–Stokes equations in the subdomains with the coupling condition

$$[\boldsymbol{\sigma}\mathbf{n}]_\Gamma = \tau\mathscr{K}\mathbf{n}$$

at the interface, i.e., the surface tension balances the jump of the normal stress on the interface. We use the notation $[v]_\Gamma = \lim_{\mathbf{x}\to\Gamma}(v_{|\Omega_2}(\mathbf{x}) - v_{|\Omega_1}(\mathbf{x}))$ for the jump across Γ, $\mathbf{n} = \mathbf{n}_\Gamma$ is the unit normal at the interface Γ (pointing from Ω_1 into Ω_2), $\mathscr{K}$ the curvature of Γ and $\boldsymbol{\sigma}$ the stress tensor defined by

$$\boldsymbol{\sigma} = -p\mathbf{I} + \mu\mathbf{D}(\mathbf{u}), \quad \mathbf{D}(\mathbf{u}) = \nabla\mathbf{u} + (\nabla\mathbf{u})^{\mathrm{T}}$$

with $p = p(\mathbf{x}, t)$ the pressure, $\mathbf{u} = \mathbf{u}(\mathbf{x}, t)$ the velocity and μ the viscosity. We assume continuity of $\mathbf{u}$ across the interface. Combined with the conservation laws for mass and momentum we obtain the following standard model, cf. for example [4–7],

$$\begin{cases} \rho_i\mathbf{u}_t - \operatorname{div}(\mu_i\mathbf{D}(\mathbf{u})) + \rho_i(\mathbf{u}\cdot\nabla)\mathbf{u} - \nabla p = \rho_i\mathbf{g} & \text{in } \Omega_i \times [0,T] \\ \operatorname{div}\mathbf{u} = 0 & \text{in } \Omega_i \times [0,T] \end{cases} \quad \text{for } i = 1,2 \tag{1.1}$$

$$[\boldsymbol{\sigma}\mathbf{n}]_\Gamma = \tau\mathscr{K}\mathbf{n}, \quad [\mathbf{u}]_\Gamma = 0. \tag{1.2}$$

The constants μ_i, ρ_i denote viscosity and density in the subdomain Ω_i, $i = 1, 2$, and $\mathbf{g}$ is an external volume force (gravity). To make this problem well-posed we need suitable boundary conditions for $\mathbf{u}$ and an initial condition $\mathbf{u}(\mathbf{x}, 0)$.

The location of the interface $\Gamma(t)$ is in general unknown and is coupled to the local flow field which transports the interface. Various approaches are used for approximating the interface. Most of these can be classified as either front-tracking or front-capturing techniques. In this paper, we use a level set method [8–10] for capturing the interface.

The two Navier–Stokes equations in Ω_i, $i = 1, 2$, in (1.1) together with the interfacial condition (1.2) can be reformulated in *one* Navier–Stokes equation on the whole domain Ω with an additional force term localized at the interface, the so-called continuum surface force (CSF) model [11,8]. We restrict ourselves to the stationary case and to homogeneous Dirichlet boundary conditions, i.e., $\mathbf{u} = 0$ on $\partial\Omega$. For a weak formulation of this problem (as in, for example [12–16]) we introduce the spaces

$$\mathbf{V} := H_0^1(\Omega)^3, \qquad Q := L_0^2(\Omega) = \left\{ q \in L^2(\Omega) \middle| \int_\Omega q\,\mathrm{d}x = 0 \right\}.$$

The standard $L^2(\Omega)$ scalar product is denoted by $(\cdot,\cdot)$ and for the Sobolev norm in $\mathbf{V}$ we use the notation $\|\cdot\|_1$. The weak formulation of the stationary CSF model is as follows: determine $(\mathbf{u}, p) \in \mathbf{V} \times Q$ such that for all $\mathbf{v} \in \mathbf{V}$ and all $q \in Q$

$$\begin{aligned} &\int_\Omega \frac{\mu}{2}\mathbf{D}(\mathbf{u}) : \mathbf{D}(\mathbf{v})\,\mathrm{d}x + (\rho\mathbf{u}\cdot\nabla\mathbf{u}, \mathbf{v}) + (\operatorname{div}\mathbf{v}, p), = (\rho\mathbf{g}, \mathbf{v}) + f_\Gamma(\mathbf{v}), \\ &(\operatorname{div}\mathbf{u}, q) = 0 \end{aligned} \tag{1.3}$$

holds, with

$$f_\Gamma(\mathbf{v}) := \tau\int_\Gamma \mathscr{K}\mathbf{n}_\Gamma \cdot \mathbf{v}\,\mathrm{d}s \tag{1.4}$$

the localized surface tension force and $\mathbf{D}(\mathbf{u}) : \mathbf{D}(\mathbf{v}) = \operatorname{tr}(\mathbf{D}(\mathbf{u})\mathbf{D}(\mathbf{v}))$. The functions μ and ρ are strictly positive and piecewise constant in $\Omega_i, i = 1, 2$, with values $\mu = \mu_i, \rho = \rho_i$ in Ω_i. For Γ sufficiently smooth we have $\sup_{x\in\Gamma}|\mathscr{K}(x)| \leqslant c < \infty$ and

$$|f_\Gamma(\mathbf{v})| \leqslant c\tau \int_\Gamma |\mathbf{n}_\Gamma \cdot \mathbf{v}| \,\mathrm{d}s \leqslant c\|\mathbf{v}\|_{L^2(\Gamma)} \leqslant c\|\mathbf{v}\|_1 \quad \text{for all } \mathbf{v} \in \mathbf{V}. \tag{1.5}$$

Thus $f_\Gamma \in \mathbf{V}'$ holds and hence (1.3) is well-defined. Under the usual assumptions (cf. [17]) the weak formulation of the Navier–Stokes equations as in (1.3) has a unique solution. Due to the Laplace–Young law, typically the pressure has a jump across the interface, when surface tension forces are present ($\tau \neq 0$), cf. Remark 1.1 below. In numerical simulations, this discontinuity and inadequate approximation of the localized surface force term often lead to strong unphysical oscillations of the velocity vector at the interface, so-called spurious velocities. In this paper, we present an alternative finite element discretization approach which significantly reduces the size of these spurious velocities compared to known standard methods. For the motivation and analysis of our approach we further simplify (1.3) and consider a Stokes problem with a constant viscosity ($\mu_1 = \mu_2 = \mu$ in Ω). We emphasize, however, that the methods that we present are *not* restricted to this simplified problem but apply to the general Navier–Stokes model (1.3) as well. We introduce the following Stokes problem: find $(\mathbf{u}, p) \in \mathbf{V} \times Q$ such that

$$\begin{aligned} &a(\mathbf{u}, \mathbf{v}) + b(\mathbf{v}, p) = (\rho \mathbf{g}, \mathbf{v}) + f_\Gamma(\mathbf{v}) \quad \text{for all } \mathbf{v} \in \mathbf{V}, \\ &b(\mathbf{u}, q) = 0 \quad \text{for all } q \in Q, \end{aligned} \tag{1.6}$$

where

$$a(\mathbf{u}, \mathbf{v}) := \int_\Omega \mu \nabla \mathbf{u} \nabla \mathbf{v} \,\mathrm{d}x, \qquad b(\mathbf{v}, q) = \int_\Omega q \,\mathrm{div}\, \mathbf{v} \,\mathrm{d}x$$

with a viscosity $\mu > 0$ that is constant in Ω. The unique solution of this problem is denoted by $(\mathbf{u}^*, p^*) \in \mathbf{V} \times Q$.

Remark 1.1. The problem (1.6) has a *smooth* velocity solution $\mathbf{u}^* \in (H^2(\Omega))^3 \cap \mathbf{V}$ and a *piecewise smooth* pressure solution p with $p_{|\Omega_i} \in H^1(\Omega_i), i = 1, 2$, which has a jump across Γ. These smoothness properties can be derived as follows. The curvature $\mathscr{K}$ is a smooth function (on Γ). Thus there exists $\hat{p}_1 \in H^1(\Omega_1)$ such that $(\hat{p}_1)_{|\Gamma} = \mathscr{K}$ (in the sense of traces). Define $\hat{p} \in L^2(\Omega)$ by $\hat{p} = \hat{p}_1$ in Ω_1, $\hat{p} = 0$ on Ω_2. Note that for all $\mathbf{v} \in \mathbf{V}$,

$$f_\Gamma(\mathbf{v}) = \tau \int_\Gamma \mathscr{K} \mathbf{n}_\Gamma \cdot \mathbf{v} \,\mathrm{d}s = \tau \int_\Gamma \hat{p}_1 \mathbf{n}_\Gamma \cdot \mathbf{v} \,\mathrm{d}s = \tau \int_{\Omega_1} \hat{p}_1 \,\mathrm{div}\, \mathbf{v} \,\mathrm{d}x + \tau \int_{\Omega_1} \nabla \hat{p}_1 \cdot \mathbf{v} \,\mathrm{d}x = \tau \int_\Omega \hat{p} \,\mathrm{div}\, \mathbf{v} \,\mathrm{d}x + \tau \int_\Omega \tilde{\mathbf{g}} \cdot \mathbf{v} \,\mathrm{d}x$$

with $\tilde{\mathbf{g}} \in L^2(\Omega)^3$ given by $\tilde{\mathbf{g}} = \nabla \hat{p}_1$ in Ω_1, $\tilde{\mathbf{g}} = 0$ on Ω_2. Thus $(\mathbf{u}^*, p^* - \tau\hat{p})$ satisfies the standard Stokes equations

$$\begin{aligned} &a(\mathbf{u}^*, \mathbf{v}) + b(\mathbf{v}, p^* - \tau\hat{p}) = (\rho \mathbf{g} + \tau \tilde{\mathbf{g}}, \mathbf{v}) \quad \text{for all } \mathbf{v} \in \mathbf{V}, \\ &b(\mathbf{u}^*, q) = 0 \quad \text{for all } q \in Q. \end{aligned}$$

From regularity results on Stokes equations and the fact that Ω is convex we conclude that $\mathbf{u}^* \in H^2(\Omega) \cap H^1_0(\Omega)$ and $p^* - \tau\hat{p} \in H^1(\Omega)$. Thus $[p^* - \tau\hat{p}]_\Gamma = 0$ (a.e. on Γ) holds, which implies

$$[p^*]_\Gamma = \tau [\hat{p}]_\Gamma = -\tau \mathscr{K},$$

i.e., p^* has a jump across Γ of the size $\tau\mathscr{K}$.

Example 1.2. A simple example, that is used in the numerical experiments in Section 4 is the following. Let $\Omega := (-1, 1)^3$ and Ω_1 a sphere with centre at the origin and radius $r < 1$. We take $\mathbf{g} = 0$. In this case, the curvature is constant, $\mathscr{K} = \frac{2}{r}$, and the solution of the Stokes problem (1.6) is given by $\mathbf{u}^* = 0$, $p^* = \tau\frac{2}{r} + c_0$ on Ω_1, $p^* = c_0$ on Ω_2 with a constant c_0 such that $\int_\Omega p^* \,\mathrm{d}x = 0$.

In the remainder of this paper, we discuss finite element discretization methods for the problem (1.6). We use a stable family $\{\mathscr{T}_h\}_{h>0}$ of consistent (i.e., no hanging nodes) nested triangulations, consisting of tetrahedra. For the evaluation of the surface tension force term $f_\Gamma(\mathbf{v})$ and of $(\rho\mathbf{g}, \mathbf{v})$ one needs the location of the interface Γ (note that $\rho = \rho_i$ is piecewise constant). The interface is approximated by a piecewise planar surface Γ_h, which is the zero level of an approximation ϕ_h of the continuous level set function ϕ, cf. Section 2.1 for more details. Once Γ_h is known we can use a stable finite element pair (e.g. Hood–Taylor) for the discret-

ization of the Stokes problem (1.6). We will show that, even for a relatively simple problem as in Example 1.2, this approach is *not* satisfactory. The discretization error (velocity in $\|\cdot\|_1$, pressure in $\|\cdot\|_{L^2}$) turns out to be proportional to $\sqrt{h}$. This rather slow convergence (for $h \downarrow 0$) is caused by two effects, namely a poor approximation of $f_\Gamma(\mathbf{v})$ and the use of a pressure finite element space that does not allow jumps in the pressure across Γ_h. The former effect has been analyzed in another paper [1]. The analysis in [1] results in an improved approximation of $f_\Gamma(\mathbf{v})$ as outlined in Section 2.1. The main topic of this paper is the introduction of an improved pressure finite element space to eliminate the second effect that causes the poor $\sqrt{h}$ convergence behaviour. This so-called extended finite element (XFEM) space is explained in Section 3. In Section 4, results of numerical experiments are presented that show a significant improvement of the discretization method (errors $\sim h^\alpha$ with $\alpha \geqslant 1$ instead of $\sqrt{h}$), provided *both* the improved treatment of $f_\Gamma(\mathbf{v})$ and the extended pressure finite element space are used. The extended finite element method is presented in [2]. In that paper, the method is applied to problems from solid mechanics. We do not know of any paper, where for a two-phase flow problem the XFEM is applied for the pressure discretization in combination with level set interface capturing and a Laplace–Beltrami approximation of the surface tension force f_Γ.

2. Discretization methods

Let $\{\mathscr{T}_h\}_{h>0}$ be a stable family of consistent (i.e., no hanging nodes) nested triangulations, consisting of tetrahedra. These triangulations are locally refined close to the interface Γ, cf. Section 4. Let $\mathbf{V}_h \subset \mathbf{V}$, $Q_h \subset Q$ be a stable pair of finite element spaces. We assume that a piecewise planar surface Γ_h is known, such that

$$\operatorname{dist}(\Gamma, \Gamma_h) \leqslant c h_\Gamma^2 \tag{2.1}$$

with h_Γ the size (diameter) of the tetrahedra in the locally refined region that contains the interface. This assumption is reasonable if one uses piecewise quadratic finite elements for the discretization of the level set function, cf. [1]. Note that in general the faces of Γ_h are not aligned with the tetrahedral triangulation $\mathscr{T}_h$, cf. Fig. 1. The induced polyhedral approximations of the subdomains are $\Omega_{1,h} = \operatorname{int}(\Gamma_h)$ (region in the interior of Γ_h) and $\Omega_{2,h} = \Omega \setminus \overline{\Omega}_{1,h}$. Furthermore, we define the piecewise constant approximation of the density ρ_h by $\rho_h = \rho_i$ on $\Omega_{i,h}$. We assume that for $\mathbf{v}_h \in \mathbf{V}_h$ the integrals in

$$(\rho_h \mathbf{g}, \mathbf{v}_h) = \rho_1 \int_{\Omega_{1,h}} \mathbf{g} \cdot \mathbf{v}_h \,\mathrm{d}x + \rho_2 \int_{\Omega_{2,h}} \mathbf{g} \cdot \mathbf{v}_h \,\mathrm{d}x$$

can be computed with high accuracy. This can be realized efficiently in our implementation because if one applies the standard finite element assembling strategy by using a loop over all tetrahedra $T \in \mathscr{T}_h$, then $T \cap \Omega_{i,h}$ is either empty or T or a relatively simple polygonal subdomain (due to the construction of Γ_h, cf. [18]).

The discretization of (1.6) is as follows: determine $(\mathbf{u}_h, p_h) \in \mathbf{V}_h \times Q_h$ such that

$$\begin{aligned} &a(\mathbf{u}_h, \mathbf{v}_h) + b(\mathbf{v}_h, p_h) = (\rho_h \mathbf{g}, \mathbf{v}_h) + f_{\Gamma_h}(\mathbf{v}_h) \quad \text{for all } \mathbf{v}_h \in \mathbf{V}_h, \\ &b(\mathbf{u}_h, q_h) = 0 \quad \text{for all } q_h \in Q_h. \end{aligned} \tag{2.2}$$

The approximation $f_{\Gamma_h}(\mathbf{v}_h)$ of $f_\Gamma(\mathbf{v}_h)$ is discussed in Section 2.1. Using standard finite element error analysis (Strang lemma) we get a discretization error bound. In our applications, we are particularly interested in problems with $\mu \ll 1$. Therefore, in the next theorem we give a discretization error bound that shows the dependence on μ.

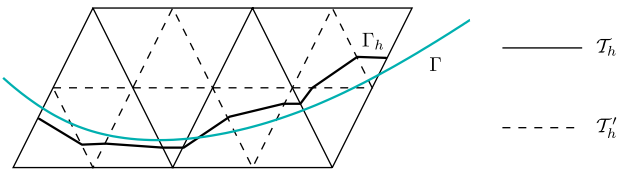

Fig. 1. Construction of approximate interface for 2D case.

Theorem 2.1. *Let* $(\mathbf{u}^*, p^*)$, $(\mathbf{u}_h, p_h)$ *be the solution of* (1.6) *and* (2.2), *respectively. Then the error bound*

$$\mu\|\mathbf{u}_h - \mathbf{u}^*\|_1 + \|p_h - p^*\|_{L^2} \leqslant c\left(\mu \inf_{\mathbf{v}_h\in\mathbf{V}_h} \|\mathbf{v}_h - \mathbf{u}^*\|_1 + \inf_{q_h\in Q_h} \|q_h - p^*\|_{L^2} + \sup_{\mathbf{v}_h\in\mathbf{V}_h} \frac{|(\rho\mathbf{g}, \mathbf{v}_h) - (\rho_h\mathbf{g}, \mathbf{v}_h)|}{\|\mathbf{v}_h\|_1} + \sup_{\mathbf{v}_h\in\mathbf{V}_h} \frac{|f_\Gamma(\mathbf{v}_h) - f_{\Gamma_h}(\mathbf{v}_h)|}{\|\mathbf{v}_h\|_1}\right) \tag{2.3}$$

holds with a constant c *independent of* h, μ *and* ρ.

Proof. The result follows from a scaling argument. For $f \in \mathbf{V}'$, $f_h \in \mathbf{V}_h'$ let $(\hat{\mathbf{u}}, \hat{p})$, $(\hat{\mathbf{u}}_h, \hat{p}_h)$ be the solutions of the μ-independent Stokes problems

$$\begin{aligned} &\int_\Omega \nabla\hat{\mathbf{u}}\nabla\mathbf{v}\,\mathrm{d}x + b(\mathbf{v}, \hat{p}) = f(\mathbf{v}) \quad \text{for all } \mathbf{v} \in \mathbf{V}, \\ &b(\hat{\mathbf{u}}, q) = 0 \quad \text{for all } q \in Q, \end{aligned} \tag{2.4}$$

$$\begin{aligned} &\int_\Omega \nabla\hat{\mathbf{u}}_h\nabla\mathbf{v}_h\,\mathrm{d}x + b(\mathbf{v}_h, \hat{p}_h) = f_h(\mathbf{v}_h) \quad \text{for all } \mathbf{v}_h \in \mathbf{V}_h, \\ &b(\hat{\mathbf{u}}_h, q_h) = 0 \quad \text{for all } q_h \in Q_h. \end{aligned} \tag{2.5}$$

Standard error analysis for Stokes equations, using the Strang lemma, yields

$$\|\hat{\mathbf{u}}_h - \hat{\mathbf{u}}\|_1 + \|\hat{p}_h - \hat{p}\|_{L^2} \leqslant c\left(\inf_{\mathbf{v}_h\in\mathbf{V}_h} \|\mathbf{v}_h - \hat{\mathbf{u}}\|_1 + \inf_{q_h\in Q_h} \|q_h - \hat{p}\|_{L^2} + \sup_{\mathbf{v}_h\in\mathbf{V}_h} \frac{|f(\mathbf{v}_h) - f_h(\mathbf{v}_h)|}{\|\mathbf{v}_h\|_1}\right) \tag{2.6}$$

with a constant c independent of f, f_h and h. Now note that $(\mathbf{u}^*, p^*)$ satisfies (2.4) with $\hat{\mathbf{u}} = \mathbf{u}^*$, $\hat{p} = \frac{1}{\mu}p^*$, $f(\mathbf{v}) = \frac{1}{\mu}((\rho\mathbf{g}, \mathbf{v}) + f_\Gamma(\mathbf{v}))$ and $(\mathbf{u}_h, p_h)$ satisfies (2.5) with $\hat{\mathbf{u}}_h = \mathbf{u}_h$, $\hat{p}_h = \frac{1}{\mu}p_h$, $f_h(\mathbf{v}_h) = \frac{1}{\mu}((\rho_h\mathbf{g}, \mathbf{v}_h) + f_{\Gamma_h}(\mathbf{v}_h))$. The result in (2.6) then yields (2.3). □

Remark 2.2. We assume Ω to be convex and thus the Stokes problem in (2.4) is H^2-regular. Using a standard duality argument it follows that $\|\hat{\mathbf{u}} - \hat{\mathbf{u}}_h\|_{L_2} \leqslant ch\|\hat{\mathbf{u}} - \hat{\mathbf{u}}_h\|_1$ and hence, due to $\hat{\mathbf{u}} = \mathbf{u}^*$, $\hat{\mathbf{u}}_h = \mathbf{u}_h$ (cf. proof of Theorem 2.1) we get

$$\|\mathbf{u}^* - \mathbf{u}_h\|_{L_2} \leqslant ch\|\mathbf{u}^* - \mathbf{u}_h\|_1$$

with a constant c independent of μ and h.

Corollary 2.3. *Let* $(\mathbf{u}^*, p^*)$, $(\mathbf{u}_h, p_h)$ *be as in Theorem* 2.1 *and define*

$$r_h := \sup_{\mathbf{v}_h\in\mathbf{V}_h} \frac{|(\rho\mathbf{g}, \mathbf{v}_h) - (\rho_h\mathbf{g}, \mathbf{v}_h)|}{\|\mathbf{v}_h\|_1} + \sup_{\mathbf{v}_h\in\mathbf{V}_h} \frac{|f_\Gamma(\mathbf{v}_h) - f_{\Gamma_h}(\mathbf{v}_h)|}{\|\mathbf{v}_h\|_1}.$$

The following holds:

$$\|\mathbf{u}_h - \mathbf{u}^*\|_1 \leqslant c\left(\inf_{\mathbf{v}_h\in\mathbf{V}_h} \|\mathbf{v}_h - \mathbf{u}^*\|_1 + \frac{1}{\mu}\inf_{q_h\in Q_h} \|q_h - p^*\|_{L^2} + \frac{1}{\mu}r_h\right), \tag{2.7}$$

$$\|\mathbf{u}_h - \mathbf{u}^*\|_{L_2} \leqslant ch\left(\inf_{\mathbf{v}_h\in\mathbf{V}_h} \|\mathbf{v}_h - \mathbf{u}^*\|_1 + \frac{1}{\mu}\inf_{q_h\in Q_h} \|q_h - p^*\|_{L^2} + \frac{1}{\mu}r_h\right), \tag{2.8}$$

$$\|p_h - p^*\|_{L^2} \leqslant c\left(\mu \inf_{\mathbf{v}_h\in\mathbf{V}_h} \|\mathbf{v}_h - \mathbf{u}^*\|_1 + \inf_{q_h\in Q_h} \|q_h - p^*\|_{L^2} + r_h\right) \tag{2.9}$$

with constants c *independent of* h, μ *and* ρ. *We observe that if* $\mu \ll 1$ *then in the velocity error we have an error amplification effect proportional to* $\frac{1}{\mu}$. *This effect does not occur in the discretization error of the pressure, cf. Remark* 4.2 *at the end of the paper.*

We comment on the terms occuring in the bound in (2.3). As explained above (Remark 1.1), the solution $\mathbf{u}^*$ of (1.6) is smooth and thus with standard finite element spaces $\mathbf{V}_h$ for the velocity (e.g. P_1 or P_2) we obtain $\inf_{\mathbf{v}_h\in\mathbf{V}_h}\|\mathbf{v}_h-\mathbf{u}^*\|_1 \leqslant ch$. Due to (2.1) we get $|\mathrm{vol}(\Omega_i)-\mathrm{vol}(\Omega_{i,h})|\leqslant ch_\Gamma^2$, $i=1,2$, and using this we obtain

$$|(\rho\mathbf{g},\mathbf{v}_h)-(\rho_h\mathbf{g},\mathbf{v}_h)| \leqslant \sum_{i=1}^{2}\rho_i\left|\int_{\Omega_i}\mathbf{g}\cdot\mathbf{v}_h\,\mathrm{d}x-\int_{\Omega_{i,h}}\mathbf{g}\cdot\mathbf{v}_h\,\mathrm{d}x\right| \leqslant c(\rho_1+\rho_2)h_\Gamma\|\mathbf{v}_h\|_1,$$

and thus an $\mathcal{O}(h_\Gamma)$ bound for the third term in (2.3). The remaining two terms in (2.3) are less easy to handle. In Section 2.1, we treat the fourth term. It is shown that a (not so obvious) approximation method based on a Laplace–Beltrami representation results in a $\mathcal{O}(h_\Gamma)$ bound for this term. The second term in (2.3) is discussed in Section 2.2. It is shown that standard finite element spaces (e.g. P_0 or P_1) lead to an error $\inf_{q_h\in Q_h}\|q_h-p^*\|_{L^2}\sim\sqrt{h_\Gamma}$. This motivates the use of another pressure finite element space, as explained in Section 3, which has much better approximation properties for functions that are piecewise smooth but discontinuous across Γ_h.

Remark 2.4. Consider the problem as in Example 1.2. Then $\mathbf{u}^*=0$, $\mathbf{g}=0$ and the bound in (2.3) simplifies to

$$\mu\|\mathbf{u}_h\|_1+\|p_h-p^*\|_{L^2}\leqslant c\left(\inf_{q_h\in Q_h}\|q_h-p^*\|_{L^2}+\sup_{\mathbf{v}_h\in\mathbf{V}_h}\frac{|f_\Gamma(\mathbf{v}_h)-f_{\Gamma_h}(\mathbf{v}_h)|}{\|\mathbf{v}_h\|_1}\right). \tag{2.10}$$

2.1. Laplace–Beltrami approximation of $f_\Gamma(\mathbf{v})$

In this section, we explain how the polyhedral approximation Γ_h of Γ is constructed and how, using Γ_h, the localized force term $f_\Gamma(\mathbf{v})$ is approximated.

The level set equation for ϕ (signed distance function) is discretized with continuous piecewise quadratic finite elements on the tetrahedral triangulation $\mathscr{T}_h$. The piecewise *quadratic* finite element approximation of ϕ on $\mathscr{T}_h$ is denoted by ϕ_h. We now introduce one further regular refinement of $\mathscr{T}_h$, resulting in $\mathscr{T}_h'$. Let $I(\phi_h)$ be the continuous piecewise *linear* function on $\mathscr{T}_h'$ which interpolates ϕ_h at all vertices of all tetrahedra in $\mathscr{T}_h'$. The approximation of the interface Γ is defined by

$$\Gamma_h := \{\mathbf{x}\in\Omega \mid I(\phi_h)(\mathbf{x})=0\} \tag{2.11}$$

and consists of piecewise planar segments. The mesh size parameter h is the maximal diameter of these segments. This maximal diameter is approximately the maximal diameter of the tetrahedra in $\mathscr{T}_h'$ that contain the discrete interface, i.e., $h=h_\Gamma$ is approximately the maximal diameter of the tetrahedra in $\mathscr{T}_h'$ *that are close to the interface*. In Fig. 1, we illustrate this construction for the two-dimensional case.

Each of the planar segments of Γ_h is either a triangle or a quadrilateral. The quadrilaterals can (formally) be divided into two triangles. Thus Γ_h consists of a set of triangular faces. Related to assumption (2.1) we note the following. If we assume $|I(\phi_h)(\mathbf{x})-\phi(\mathbf{x})|\leqslant ch_\Gamma^2$ for all $\mathbf{x}$ in a neighbourhood of Γ, which is reasonable for a smooth ϕ and piecewise quadratic ϕ_h, then we have

$$\mathrm{dist}(\Gamma,\Gamma_h)=\max_{\mathbf{x}\in\Gamma_h}|\phi(\mathbf{x})|=\max_{\mathbf{x}\in\Gamma_h}|\phi(\mathbf{x})-I(\phi_h)(\mathbf{x})|\leqslant ch_\Gamma^2,$$

and thus (2.1) is satisfied.

The approximation of the localized surface tension force is based on a Laplace–Beltrami characterization of the curvature. For this we have to introduce some elementary notions from differential geometry. Let U be an open subset in $\mathbb{R}^3$ and Γ a connected C^2 compact hypersurface contained in U. For a sufficiently smooth function $g:U\to\mathbb{R}$ the tangential derivative (along Γ) is defined by projecting the derivative on the tangent space of Γ, i.e.

$$\nabla_\Gamma g=\nabla g-\nabla g\cdot\mathbf{n}_\Gamma\mathbf{n}_\Gamma. \tag{2.12}$$

The *Laplace–Beltrami operator* on Γ is defined by

$$\Delta_\Gamma g:=\nabla_\Gamma\cdot\nabla_\Gamma g.$$

It can be shown that $\nabla_\Gamma g$ and $\Delta_\Gamma g$ depend only on values of g on Γ. For vector valued functions $f, g : \Gamma \to \mathbb{R}^3$ we define

$$\Delta_\Gamma f := (\Delta_\Gamma f_1, \Delta_\Gamma f_2, \Delta_\Gamma f_3)^{\mathrm{T}}, \qquad \nabla_\Gamma f \cdot \nabla_\Gamma g := \sum_{i=1}^{3} \nabla_\Gamma f_i \cdot \nabla_\Gamma g_i.$$

We recall the following basic result from differential geometry.

Theorem 2.5. *Let* $\mathrm{id}_\Gamma : \Gamma \to \mathbb{R}^3$ *be the identity on* Γ *and* $\mathscr{K} = \kappa_1 + \kappa_2$ *the sum of the principal curvatures. For all sufficiently smooth vector functions* $\mathbf{v}$ *on* Γ *the following holds*:

$$\int_\Gamma \mathscr{K}\mathbf{n}_\Gamma \cdot \mathbf{v}\,\mathrm{d}s = -\int_\Gamma (\Delta_\Gamma \mathrm{id}_\Gamma) \cdot \mathbf{v}\,\mathrm{d}s = \int_\Gamma \nabla_\Gamma \mathrm{id}_\Gamma \cdot \nabla_\Gamma \mathbf{v}\,\mathrm{d}s. \tag{2.13}$$

In view of the result in this theorem an obvious choice for $f_{\Gamma_h}(\mathbf{v}_h)$ in (2.2) (that is used in, e.g. [19,20,12,18,21]) is the following:

$$f_{\Gamma_h}(\mathbf{v}_h) := \tau \int_{\Gamma_h} \nabla_{\Gamma_h} \mathrm{id}_{\Gamma_h} \cdot \nabla_{\Gamma_h} \mathbf{v}_h\,\mathrm{d}s, \quad \mathbf{v}_h \in \mathbf{V}_h. \tag{2.14}$$

Here id_{Γ_h} denotes the identity $\Gamma_h \to \mathbb{R}^3$, i.e., the coordinate vector on Γ_h. Analysis and numerical experiments in [1] yield that for this choice we have

$$\sup_{\mathbf{v}_h \in \mathbf{V}_h} \frac{|f_\Gamma(\mathbf{v}_h) - f_{\Gamma_h}(\mathbf{v}_h)|}{\|\mathbf{v}_h\|_1} \leqslant c\sqrt{h_\Gamma}, \tag{2.15}$$

and that this bound is sharp w.r.t. the order of convergence for $h_\Gamma \downarrow 0$. In view of the analysis in Section 2 this approximation error is relatively large, compared to the $\mathcal{O}(h)$ bounds for the first and third term in (2.3). In Ref. [1], a modified surface tension force discretization with better approximation quality is presented. We briefly explain this method. For this we have to introduce some further notation. Let $\boldsymbol{n}_h$ be the unit normal on Γ_h (outward pointing from $\Omega_{1,h}$). Since Γ_h is planar piecewise triangular, this normal is piecewise constant (and not defined at the edges of the surface triangulation). We define the orthogonal projection $\mathbf{P}_h$:

$$\mathbf{P}_h(\mathbf{x}) := \mathbf{I} - \mathbf{n}_h(\mathbf{x})\mathbf{n}_h(\mathbf{x})^{\mathrm{T}} \quad \text{for } \mathbf{x} \in \Gamma_h, \mathbf{x} \text{ not on an edge.}$$

Recall that the discrete level set function ϕ_h is piecewise quadratic. Define

$$\tilde{\mathbf{n}}_h(\mathbf{x}) := \frac{\nabla \phi_h(\mathbf{x})}{\|\nabla \phi_h(\mathbf{x})\|}, \qquad \tilde{\mathbf{P}}_h(\mathbf{x}) := \mathbf{I} - \tilde{\mathbf{n}}_h(\mathbf{x})\tilde{\mathbf{n}}_h(\mathbf{x})^{\mathrm{T}}, \ \mathbf{x} \in \Gamma_h, \mathbf{x} \text{ not on an edge.}$$

For the discrete surface tension force as in (2.14) we have, due to $\nabla_{\Gamma_h} g = \mathbf{P}_h \nabla g$ (for smooth functions g), the representation

$$f_{\Gamma_h}(\mathbf{v}_h) = \tau \sum_{i=1}^{3} \int_{\Gamma_h} \mathbf{P}_h(\mathbf{x})\mathbf{e}_i \cdot \nabla_{\Gamma_h} (\mathbf{v}_h)_i\,\mathrm{d}s \tag{2.16}$$

with $\boldsymbol{e}_i$ the ith basis vector in $\mathbb{R}^3$ and $(\mathbf{v}_h)_i$ the ith component of $\mathbf{v}_h$. The *modified* discrete surface tension force is given by

$$\tilde{f}_{\Gamma_h}(\mathbf{v}_h) = \tau \sum_{i=1}^{3} \int_{\Gamma_h} \tilde{\mathbf{P}}_h(\mathbf{x})\mathbf{e}_i \cdot \nabla_{\Gamma_h} (\mathbf{v}_h)_i\,\mathrm{d}s. \tag{2.17}$$

The implementation of this functional requires only a minor modification if the implementation of the one in (2.16) is available. In Ref. [1], it is shown that under reasonable assumptions on Γ_h and ϕ_h, we have the error bound

$$\sup_{\mathbf{v}_h \in \mathbf{V}_h} \frac{|f_\Gamma(\mathbf{v}_h) - \tilde{f}_{\Gamma_h}(\mathbf{v}_h)|}{\|\mathbf{v}_h\|_1} \leqslant c h_\Gamma. \tag{2.18}$$

This bound has the desired $\mathcal{O}(h_\Gamma)$ behaviour (instead of $\mathcal{O}(\sqrt{h_\Gamma})$, cf (2.15)). Numerical experiments in [1] show a rate of convergence that is even somewhat higher than first order in h_Γ.

2.2. Analysis of the term $\inf_{q_h\in Q_h}\|q_h - p^*\|_{L^2}$

In this section, we consider the approximation error $\inf_{q_h\in Q_h}\|q_h - p^*\|_{L^2}$ for a few standard finite element spaces Q_h and explain why in general for a function p^* that is discontinuous across Γ_h one can expect no better bound for this approximation error than $c\sqrt{h}$. This serves as a motivation for an improved pressure finite element space as presented in Section 3. To explain the effect underlying the $\sqrt{h}$ behaviour of the error bound we analyze a concrete two-dimensional example as illustrated in Fig. 2. We take $\Omega = (0,1)^2$ and define $\Omega_1 := \{(x,y) \in \Omega \mid x \leqslant 1 - y\}$, $\Omega_2 := \Omega \setminus \overline{\Omega}_1$. A family of triangulations $\{\mathscr{T}_h\}_{h>0}$ is constructed as follows. The starting triangulation T_0 consists of two triangles, namely the ones with vertices $\{(0,0),(0,1),(1,1)\}$ and $\{(0,0),(1,0),(1,1)\}$. Then a global regular refinement strategy (connecting the midpoints of edges) is applied repeatedly. This results in a nested sequence of triangulations T_{h_k}, $k = 1,2,\ldots$, with mesh size $h_k = 2^{-k}$. In Fig. 2, the triangulation $\mathscr{T}_{h_2}$ is shown. As interface we take $\Gamma = \{(x,y) \in \Omega \mid y = 1 - x\}$. The set of triangles that contains the interface is given by (with $h := h_k$)

$$\mathscr{T}_h^\Gamma := \{T \in \mathscr{T}_h \mid \mathrm{meas}_1(T \cap \Gamma) > 0\}.$$

In Fig. 2, the elements in $\mathscr{T}_{h_2}^\Gamma$ are colored grey.

For $h = h_k$ we consider the finite element spaces

$$Q_h^0 := \{p \mid p_{|T} \in \mathscr{P}_0 \quad \text{for all } T \in \mathscr{T}_h\} \quad \text{(piecewise constants)},$$
$$Q_h^{1,\mathrm{disc}} := \{p \mid p_{|T} \in \mathscr{P}_1 \quad \text{for all } T \in \mathscr{T}_h\} \quad \text{(piecewise linears, discontinuous)},$$
$$Q_h^1 := \{p \in C(\Omega) \mid p_{|T} \in \mathscr{P}_1 \quad \text{for all } T \in \mathscr{T}_h\} \quad \text{(piecewise linears, continuous)}.$$

Note that

$$Q_h^j \subset Q_h^{1,\mathrm{disc}} \quad \text{for } j = 0,1. \tag{2.19}$$

We take p^* as follows: $p^*(x,y) = c_p > 0$ for all $(x,y) \in \Omega_1$, $p(x,y) = 0$ for all $(x,y) \in \Omega_2$. We study $\inf_{q_h\in Q_h}\|q_h - p^*\|_{L^2}$ for $Q_h \in \{Q_h^0, Q_h^{1,\mathrm{disc}}, Q_h^1\}$. For $Q_h = Q_h^{1,\mathrm{disc}}$ the identity

$$\inf_{q_h\in Q_h^{1,\mathrm{disc}}} \|q_h - p^*\|_{L^2}^2 = \sum_{T\in\mathscr{T}_h^\Gamma} \min_{q\in\mathscr{P}_1} \|q - p^*\|_{L^2(T)}^2$$

holds. Take $T \in \mathscr{T}_h^\Gamma$. Using a quadrature rule on triangles that is exact for all polynomials of degree two we get, cf. Fig. 2,

$$\begin{aligned}
\min_{q\in\mathscr{P}_1} \|q - p^*\|_{L^2(T)}^2 &= \min_{q\in\mathscr{P}_1} \left(\int_{T_L} (q - c_p)^2 \,\mathrm{d}x\,\mathrm{d}y + \int_{T_U} q^2 \,\mathrm{d}x\,\mathrm{d}y \right) \\
&= \frac{1}{12} h^2 \min_{q\in\mathscr{P}_1} \left((q(m_3) - c_p)^2 + (q(m_4) - c_p)^2 + (q(m) - c_p)^2 + q(m_1)^2 + q(m_2)^2 + q(m)^2 \right) \\
&\geqslant \frac{1}{12} h^2 \min_{q\in\mathscr{P}_1} \left((q(m) - c_p)^2 + q(m)^2 \right) = \frac{1}{24} c_p^2 h^2.
\end{aligned}$$

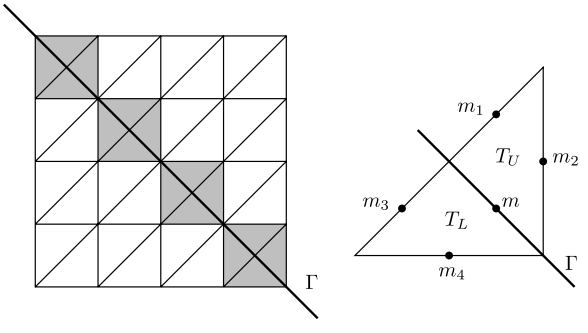

Fig. 2. Triangulation T_{h_2} and a triangle $T \in \mathscr{T}_{h_k}^\Gamma$.

Thus we have

$$\inf_{q_h\in Q_h^{1,\mathrm{disc}}} \|q_h - p^*\|_{L^2} \geqslant \left(\sum_{T\in\mathscr{T}_h^\Gamma} \frac{1}{24}c_p^2h^2\right)^{\frac{1}{2}} = \left(\frac{2}{h}\frac{1}{24}c_p^2h^2\right)^{\frac{1}{2}} = \frac{1}{2\sqrt{3}}c_p\sqrt{h}.$$

Due to (2.19) this yields

$$\inf_{q_h\in Q_h} \|q_h - p^*\|_{L^2} \geqslant \frac{1}{2\sqrt{3}}c_p\sqrt{h} \quad \text{for } Q_h \in \{Q_h^0, Q_h^{1,\mathrm{disc}}, Q_h^1\}. \tag{2.20}$$

To derive an upper bound for the approximation error we choose a suitable $q_h \in Q_h$. First consider $Q_h = Q_h^0$ and take $q_h^0 \in Q_h^0$ as follows: $(q_h^0)_{|T} = c_p$ for all T with $\mathrm{meas}_1(T\cap\Omega_1) > 0$, $q_h^0 = 0$ otherwise. With this choice we get

$$\|q_h^0 - p^*\|_{L^2} = \left(\underset{T\in\mathscr{T}_h^\Gamma}{m}\|q_h^0 - p^*\|_{L^2(T)}^2\right)^{\frac{1}{2}} = \left(\sum_{T\in\mathscr{T}_h^\Gamma} c_p^2\frac{1}{4}h^2\right)^{\frac{1}{2}} = \frac{1}{\sqrt{2}}c_p\sqrt{h}. \tag{2.21}$$

For $Q_h = Q_h^1$ we take $q_h^1 := I_h(p^*)$, where I_h is the nodal interpolation operator (note: $p^* = c_p$ on Γ). Elementary computations yield

$$\|q_h^1 - p^*\|_{L^2} = \left(\frac{1}{12}c_p^2h\right)^{\frac{1}{2}} = \frac{1}{2\sqrt{3}}c_p\sqrt{h}. \tag{2.22}$$

Combination of (2.19)–(2.22) yields

$$\frac{1}{2\sqrt{3}}c_p\sqrt{h} \leqslant \inf_{q_h\in Q_h} \|q_h - p^*\|_{L^2} \leqslant \frac{1}{\sqrt{2}}c_p\sqrt{h} \quad \text{for } Q_h \in \{Q_h^0, Q_h^{1,\mathrm{disc}}, Q_h^1\}. \tag{2.23}$$

Note that this approximation error result does not change if we apply only *local* refinement close to the interface and then replace h by h_Γ, where the latter denotes the mesh size of the triangles in $\mathscr{T}_h^\Gamma$.

If instead of piecewise constants or piecewise linears we consider polynomials of higher degree, the approximation error still behaves like $\sqrt{h}$.

Similar examples, which have a $\sqrt{h}$ approximation error behaviour, can be constructed using these finite element spaces on tetrahedral triangulations in 3D.

3. Extended finite element space for the pressure

The analysis in the previous section, which is confirmed by numerical experiments in Section 4, leads to the conclusion that there is a need for an improved finite element space for the pressure. In this section, we present such a space which is based on an idea presented in [2,3]. In that paper, a so-called extended finite element space (XFEM) is introduced which has good approximation properties for interface type of problems.

Here we apply the XFEM method to two-phase flow problems by constructing an extended pressure finite element space Q_h^Γ. In this section, we explain the method and discuss some implementation issues. In Section 4, results of numerical experiments with this method are presented.

For $k \geqslant 1$ fixed we introduce the standard finite element space

$$Q_h = Q_h^k = \{q \in C(\Omega)\cap L_0^2(\Omega) \mid q|_T \in \mathscr{P}_k \quad \text{for all } T \in \mathscr{T}\}.$$

For $k = 1$, for example, this is the standard finite element space of continuous piecewise linear functions. We define the index set $\mathscr{J} = \{1,\ldots,n\}$, where $n = \dim Q_h$ is the number of degrees of freedom. Let $\mathscr{B} := \{q_j\}_{j=1}^n$ be the nodal basis of Q_h, i.e. $q_j(\mathbf{x}_i) = \delta_{i,j}$ for $i,j \in \mathscr{J}$ where $\mathbf{x}_i \in \mathbb{R}^3$ denotes the spatial coordinate of the ith degree of freedom.

The idea of the XFEM method is to enrich the original finite element space Q_h by additional basis functions q_j^X for $j \in \mathscr{J}'$ where $\mathscr{J}' \subset \mathscr{J}$ is a given index set. An additional basis function q_j^X is constructed by multiplying the original nodal basis function q_j by a so-called enrichment function Φ_j:

$$q_j^X(\mathbf{x}) := q_j(\mathbf{x})\Phi_j(\mathbf{x}). \tag{3.1}$$

This enrichment yields the extended finite element space

$$Q_h^X := \operatorname{span}\left(\{q_j\}_{j\in\mathscr{J}} \cup \{q_j^X\}_{j\in\mathscr{J}'}\right).$$

This idea was introduced in [2] and further developed in [3] for different kinds of discontinuities (kinks, jumps), which may also intersect or branch. The choice of the enrichment function depends on the type of discontinuity. For representing jumps the Heaviside function is proposed to construct appropriate enrichment functions. Basis functions with kinks can be obtained by using the distance function as enrichment function.

In our case, the finite element space Q_h^1 is enriched by discontinuous basis functions q_j^X for $j \in \mathscr{J}' = \mathscr{J}_\Gamma := \{j \in \mathscr{J} \mid \operatorname{meas}_2(\Gamma \cap \operatorname{supp} q_j) > 0\}$, as discontinuities only occur at the interface. Let $d : \Omega \to \mathbb{R}$ be the signed distance function (or an approximation to it) with d negative in Ω_1 and positive in Ω_2. For example the level set function φ could be used for d. Then by means of the Heaviside function H we define

$$H_\Gamma(\mathbf{x}) := H(d(\mathbf{x})) = \begin{cases} 0 & \mathbf{x} \in \Omega_1, \\ 1 & \mathbf{x} \in \Omega_2. \end{cases}$$

As we are interested in functions with a jump across the interface we define the enrichment function

$$\Phi_j^H(\mathbf{x}) := H_\Gamma(\mathbf{x}) - H_\Gamma(\mathbf{x}_j) \tag{3.2}$$

and a corresponding function $q_j^X := q_j \cdot \Phi_j^H$, $j \in \mathscr{J}'$. The second term in the definition of Φ_j^H is constant and may be omitted (as it does not introduce new functions in the function space), but ensures the nice property $q_j^X(\mathbf{x}_i) = 0$, i.e. q_j^X vanishes in all degrees of freedom. As a consequence, we have

$$\operatorname{supp} q_j^X \subset \left(\operatorname{supp} q_j \cap \bigcup_{T\in\mathscr{T}_h^\Gamma} T\right), \tag{3.3}$$

where $\mathscr{T}_h^\Gamma = \{T \in \mathscr{T}_h \mid \operatorname{meas}_2(T \cap \Gamma) > 0\}$. Thus $q_j^X \equiv 0$ in all T with $T \notin \mathscr{T}_h^\Gamma$.

In the following, we will use the notation $q_j^\Gamma := q_j\Phi_j^H$ and

$$Q_h^\Gamma := \operatorname{span}(\{q_j | j \in \mathscr{J}\} \cup \{q_j^\Gamma | j \in \mathscr{J}_\Gamma\})$$

to emphasize that the extended finite element space Q_h^Γ depends on the location of the interface Γ. In particular, the dimension of Q_h^Γ may change if the interface is moved. The shape of the extended basis functions for the 1D case is sketched in Fig. 3.

Remark 3.1. Note that Q_h^Γ can also be characterized by the following property: $q \in Q_h^\Gamma$ if and only if there exist functions $q_1, q_2 \in Q_h$ such that $q|_{\Omega_i} = q_i|_{\Omega_i}$, $i = 1, 2$.

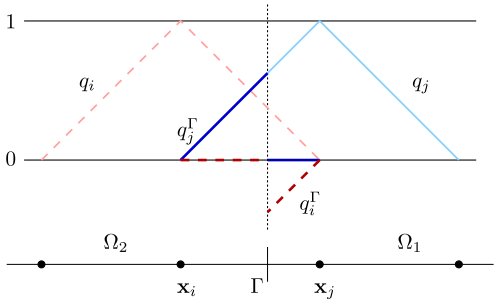

Fig. 3. Extended finite element basis functions q_i, q_i^Γ (dashed) and q_j, q_j^Γ (solid) for 1D case.

The application of this method to the solution of two-phase flow problems leads to several challenging issues which should be addressed. Theoretical questions like stability of the $\mathbf{V}_h - Q_h^\Gamma$ finite element pair or the convergence order of the method are still unanswered. For pressure solutions p with $p_{|\Omega_i} \in H^1(\Omega_i), i = 1, 2$ (cf. Remark 1.1), we expect

$$\inf_{q_h \in Q_h^\Gamma} \|q_h - p\|_{L^2} \leqslant ch.$$

This yields the desired $\mathcal{O}(h)$ bound, cf. Section 2.

An important issue from the practical point of view is the design of efficient and robust solvers for the resulting discrete problems which have to be adapted to the extended pressure finite element space. These are topics of current research, cf. Section 5.

Remark 3.2. In Ref. [3] the XFEM is applied to a few problems from linear elasticity demonstrating the ability of the method to capture jumps and kinks. These discontinuities also branch or intersect in some of the examples, in this case more elaborate constructions of the enrichment functions are used.

In Ref. [22], the XFEM is also applied to a two-phase flow problem. In that paper, discontinuous material properties ρ and μ, but *no surface tension forces* were taken into account. Thus there is no jump in pressure, but the solution exhibits kinks at the interface. For the pressure and the level set function standard finite element spaces are used. The velocity field is discretized with an extended finite element space enriched by $q_j^X(\mathbf{x}) = q_j(\mathbf{x}) \cdot |d(\mathbf{x})|$ to capture the kinks at the interface.

Remark 3.3. We comment on two related approaches that are known in the literature. In Refs. [23,24], a discontinuous finite element space V_h^{disc} is introduced and applied to a scalar elliptic interface problem, where the continuity of the solution is enforced by Lagrangian multipliers. For the construction of V_h^{disc} the standard finite element space Q_h^1 is modified by replacing each of the basis functions $q_j, j \in \mathcal{J}_\Gamma$, by the two functions

$$q_j^{\Gamma,i}(\mathbf{x}) = \begin{cases} q_j(\mathbf{x}), & x \in \Omega_i, \\ 0, & x \notin \Omega_i. \end{cases} \qquad i = 1, 2.$$

This yields the same finite element space as the XFEM approach, i.e. $V_h^{\text{disc}} = Q_h^\Gamma$, cf. Remark 3.1. In this sense the approach of Hansbo is a special case of the XFEM approach where the latter is more general as it can relatively easy be adapted to other kinds of discontinuities. In Ref. [24], an error analysis for this finite element method is presented.

In Ref. [25], the standard finite element space Q_h^1 is extended by discontinuous basis functions q_T^Γ for $T \in \mathcal{T}_h^\Gamma$, which are defined by

$$q_T^\Gamma(\mathbf{x}) := \begin{cases} H_\Gamma(\mathbf{x}) - \sum_j H_\Gamma(\mathbf{x}_j) \cdot q_j(\mathbf{x}), & \mathbf{x} \in T, \\ 0, & \text{otherwise.} \end{cases}$$

This introduces $|\mathcal{T}_h^\Gamma|$ new degrees of freedom, which influence the height of the jump in the corresponding elements. q_T^Γ is not only discontinuous across Γ but also across element boundaries (edges in 2D, faces in 3D) that intersect Γ where p^* is known to be continuous. Due to this disadvantage we did not consider this method for the approximation of discontinuous pressure in two-phase flows.

3.1. Implementation issues

Let Γ_h be a piecewise planar approximation of the interface Γ as described in Section 2.1. For practical reasons we do not consider Q_h^Γ but the space $Q_h^{\Gamma_h}$ which is much easier to construct. Here $Q_h^{\Gamma_h}$ is the extended pressure finite element space described above but with Γ replaced by its approximation Γ_h. We thus consider the finite element discretization (2.2) for the choice $Q_h = Q_h^{\Gamma_h}$. As the velocity space $\mathbf{V}_h$ is unchanged most of the terms are discretized like before. Only the evaluation of $b(\cdot,\cdot)$ requires further explanation.

For a basis function $\mathbf{v}_i \in \mathbf{V}_h$ and $j \in \mathscr{J}_\Gamma$ the evaluation of

$$b(\mathbf{v}_i, q_j^{\Gamma_h}) = \sum_{T' \in \mathscr{T}'_h} \int_{T'} q_j^{\Gamma_h} \mathrm{div}\mathbf{v}_i \, \mathrm{d}\mathbf{x}$$

requires the computation of integrals with discontinuous integrands, as the extended pressure basis function $q_j^{\Gamma_h}$ has a jump across the interface. We sum over $T' \in \mathscr{T}'_h$ (and not $T \in \mathscr{T}_h$) because Γ_h is defined as in (2.11). Let $T \in \mathscr{T}_h$ be a tetrahedron with $T \cap \mathrm{supp} q_j^{\Gamma_h} \neq \emptyset$ and $T' \in \mathscr{T}'_h$ with $T' \subset T$ a child tetrahedron created by regular refinement of T. Due to (3.3) we conclude $T \in \mathscr{T}_h^\Gamma$, and define

$$T_i := T \cap \Omega_{i,h}, \quad T'_i := T' \cap \Omega_{i,h}, \quad i = 1, 2.$$

Using the definition of $q_j^{\Gamma_h}$, cf. (3.1) and (3.2), we get

$$\int_{T'} q_j^{\Gamma_h} \mathrm{div}\mathbf{v}_i \, \mathrm{d}\mathbf{x} = \int_{T'_2} q_j \mathrm{div}\mathbf{v}_i \, \mathrm{d}\mathbf{x} - H_\Gamma(\mathbf{x}_j) \int_{T'} q_j \mathrm{div}\mathbf{v}_i \, \mathrm{d}\mathbf{x} = \begin{cases} \int_{T'_2} q_j \mathrm{div}\mathbf{v}_i \, \mathrm{d}\mathbf{x} & \text{if } \mathbf{x}_j \in \Omega_1, \\ -\int_{T'_1} q_j \mathrm{div}\mathbf{v}_i d\mathbf{x} & \text{if } \mathbf{x}_j \in \Omega_2. \end{cases} \tag{3.4}$$

The integrands in the right-hand side of (3.4) are continuous and the subdomains T'_1, T'_2 are polyhedral since by construction Γ_h consists of piecewise planar segments (cf. Section 2.1). For the computation of the integral over T'_i we distinguish two cases. The face $T' \cap \Gamma_h$ is either a triangle or a quadrilateral. In the first case one of the sets T'_1, T'_2 is tetrahedral. In the second case both T'_1, T'_2 are non-tetrahedral, but can each be subdivided into three subtetrahedra. In all cases, the integration over T'_i can be reduced to integration on tetrahedra, for which standard quadrature rules can be applied.

4. Numerical results

In this section, we consider the following Stokes problem on the domain $\Omega = (-1, 1)^3$ using the notation from Section 1

$$\begin{aligned} &a(\mathbf{u}, \mathbf{v}) + b(\mathbf{v}, p) = f_{\mathrm{SF}}(\mathbf{v}) \quad \text{for all } \mathbf{v} \in \mathbf{V}, \\ &b(\mathbf{u}, q) = 0 \quad \text{for all } q \in Q. \end{aligned} \tag{4.1}$$

Here $f_{\mathrm{SF}} \in \mathbf{V}'$ is a surface force term on the interface Γ which will be specified in the two test cases below. For simplicity we assume constant viscosity $\mu = 1$. The finite element discretization of (4.1) is as follows:

$$\begin{aligned} &a(\mathbf{u}_h, \mathbf{v}_h) + b(\mathbf{v}_h, p_h) = f_{\mathrm{SF},h}(\mathbf{v}_h) \quad \text{for all } \mathbf{v}_h \in \mathbf{V}_h, \\ &b(\mathbf{u}_h, q_h) = 0 \quad \text{for all } q_h \in Q_h, \end{aligned} \tag{4.2}$$

where $f_{\mathrm{SF},h} \in \mathbf{V}'_h$ is an approximation of f_{SF}. We choose a uniform initial triangulation $\mathscr{T}_0$ where the vertices form a $5 \times 5 \times 5$ lattice and apply an adaptive refinement algorithm presented in [26]. Local refinement of the coarse mesh $\mathscr{T}_0$ in the vicinity of Γ yields the gradually refined meshes $\mathscr{T}_1, \mathscr{T}_2, \mathscr{T}_3, \mathscr{T}_4$ with local mesh sizes $h_\Gamma = h_i = 2^{-i-1}, i = 0, \ldots, 4$ at the interface. For the discretization of $\mathbf{u}$ we choose the standard finite element space of piecewise quadratics:

$$\mathbf{V}_h := \{\mathbf{v} \in C(\Omega)^3 | \mathbf{v}|_T \in \mathscr{P}_2 \quad \text{for all } T \in \mathscr{T}_h, \ \mathbf{v}_{|\partial\Omega} = 0\}.$$

We compute the errors

$$e_{\mathbf{u}} := \mathbf{u}^* - \mathbf{u}_h \quad \text{and} \quad e_p := p^* - p_h$$

for different choices of the pressure finite element space Q_h to compare the approximation properties of the different spaces. In our experiments, we used piecewise constant or continuous piecewise linear elements, i.e. the spaces Q_h^0, Q_h^1 respectively, and the extended pressure space $Q_h^{\Gamma_h}$.

Test case A: pressure jump at a planar interface

This simple test case is designed to examine interpolation errors of finite element spaces for the approximation of discontinuous jumps of the pressure variable.

For f_{SF} we choose the artificial surface force $f_{\mathrm{SF}} = f_{\mathrm{ASF}}$ where

$$f_{\mathrm{ASF}}(\mathbf{v}) = \sigma \int_\Gamma \mathbf{v} \cdot \mathbf{n} \, \mathrm{d}s, \quad \mathbf{v} \in \mathbf{V}$$

and $\sigma > 0$ is a constant. Note that $f_{\mathrm{ASF}} \in \mathbf{V}'$. This yields the unique solution

$$\mathbf{u}^* = 0, \qquad p^* = \begin{cases} C & \text{in } \Omega_1, \\ C + \sigma & \text{in } \Omega_2. \end{cases}$$

Here C is a constant such that $\int_\Omega p^* \,\mathrm{d}x = 0$. In our calculations, we used $\sigma = 1$.

We consider two different interfaces Γ_1 and Γ_2, which are both planes. Γ_1 is defined by $\Gamma_1 = \{(x,y,z) \in \Omega \mid z = 0\}$. In this case the two subdomains are given by $\Omega_1 := \{(x,y,z) \in \Omega \mid z < 0\}$ and $\Omega_2 := \Omega \setminus \overline{\Omega}_1$, cf. Fig. 4. Interface Γ_2 is defined by $\Gamma_2 = \{(x,y,z) \in \Omega \mid y + z = 0\}$ and the subdomains $\Omega_1 := \{(x,y,z) \in \Omega \mid y + z < 0\}$ and $\Omega_2 := \Omega \setminus \overline{\Omega}_1$. We emphasize that for both interfaces the interface approximation Γ_h is exact, i.e. $\Gamma_h = \Gamma$, allowing for an exact discretization of the interfacial force, i.e. $f_{\mathrm{ASF},h} = f_{\mathrm{ASF}}$.

Due to $\mathbf{g} = 0$, $\mathbf{u}^* \in \mathbf{V}_h$ and the fact that $\|f_{\mathrm{ASF},h} - f_{\mathrm{ASF}}\|_{\mathbf{V}_h'} = 0$ the error bound (2.3) simplifies to

$$\mu \|e_{\mathbf{u}}\|_1 + \|e_p\|_{L^2} \leqslant c \inf_{q_h \in Q_h} \|p^* - q_h\|_{L^2}. \tag{4.3}$$

Thus the errors in velocity and pressure are solely controlled by the approximation property of the finite element space Q_h.

The number of velocity and pressure unknowns for the grids $\mathscr{T}_0, \ldots, \mathscr{T}_4$ with different refinement levels are shown in Table 1. Note that $\dim Q_h^{\Gamma_h} > \dim Q_h^1$ due to the extended basis functions.

Test case B: static bubble

In this test case (cf. Example 1.2) we consider a static bubble $\Omega_2 = \{x \in \mathbb{R}^3 \mid \|x\| \leqslant r\}$ in the cube Ω with $r = 2/3$ (see Fig. 5). We assume that surface tension is present, i.e. $f_{\mathrm{SF}} = f_\Gamma$ with $\tau = 1$. This problem has the unique solution

$$u^* = 0, \qquad p^* = \begin{cases} C & \text{in } \Omega_1, \\ C + \tau\mathscr{K} & \text{in } \Omega_2. \end{cases}$$

Since $\mathscr{K} = 2/r$, the pressure jump is equal to $[p^*]_\Gamma = 3$. A 2D variant of this test case is presented in [20,27].

Note that in this test case the errors in velocity and pressure are influenced by two error sources, namely the approximation error of the discontinuous pressure p^* in Q_h (as in test case A) and errors induced by the discretization of the surface force f_Γ, cf. (2.10).

Table 1
Dimensions of the finite element spaces for test cases A and B

# Ref.	Test case A, $\Gamma = \Gamma_1$				Test case A, $\Gamma = \Gamma_2$				Test case B		
	$\dim \mathbf{V}_h$	$\dim Q_h^1$	$\dim Q_h^{\Gamma_h}$	$\dim Q_h^0$	$\dim \mathbf{V}_h$	$\dim Q_h^1$	$\dim Q_h^{\Gamma_h}$	$\dim Q_h^0$	$\dim \mathbf{V}_h$	$\dim Q_h^1$	$\dim Q_h^{\Gamma_h}$
0	1029	125	150	384	1029	125	190	384	1029	125	176
1	6801	455	536	1984	7749	543	768	2304	5523	337	533
2	31,197	1657	1946	8384	42,633	2313	3146	11,556	30,297	1475	2295
3	131,433	6235	7324	33,984	200,469	9607	12,808	52,088	139,029	6127	9413
4	537,717	24,093	28,318	136,384	871,881	39,229	51,774	221,796	569,787	24,373	37,355

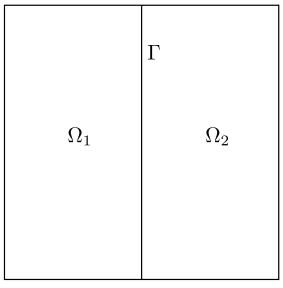

Fig. 4. 2D illustration of the computational domain $\Omega = \Omega_1 \cup \Omega_2$ and interface $\Gamma = \Gamma_1$ for test case A.

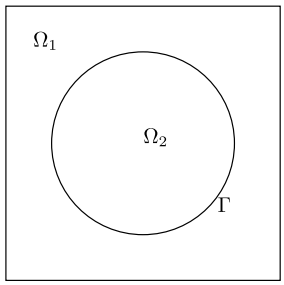

Fig. 5. 2D illustration of the computational domain $\Omega = \Omega_1 \cup \Omega_2$ and interface Γ for test case B.

The number of velocity and pressure unknowns for the grids $\mathscr{T}_0, \ldots, \mathscr{T}_4$ with different refinement levels are shown in Table 1.

Remark 4.1. As Γ has constant curvature, for $\sigma = \frac{2\tau}{r}$ the two considered surface forces coincide: $f_\Gamma = f_{\mathrm{ASF}}$.

4.1. Test case A: pressure jump at a planar interface

4.1.1. Interface at $\Gamma = \Gamma_1$

For $\Gamma = \Gamma_1$, the interface Γ is only located at the element boundaries of tetrahedra intersected by Γ, i.e. for each tetrahedron T intersecting Γ we have that $\Gamma \cap T$ is equal to a face of T.

In this special situation, the discontinuous pressure p^* can be represented exactly in the finite element space Q_h^0 of piecewise constants, thus the finite element solution $(\mathbf{u}_h, p_h) \in \mathbf{V}_h \times Q_h^0$ is equal to $(\mathbf{u}^*, p^*)$. This is confirmed by the numerical results: the exact solution $(\mathbf{u}^*, p^*)$ fulfills the discrete equations (up to round-off errors). The same holds for the extended finite element space $Q_h^{\Gamma_h}$.

For the P_1 finite elements we obviously have $p^* \notin Q_h^1$. The grid $\mathscr{T}_3$ after 3 times refinement and the corresponding pressure solution are shown in Figs. 6 and 7. The error norms for different grid refinement levels are shown in Table 2. The L^2-error of the pressure shows a decay of $\mathscr{O}(h^{1/2})$. This confirms the theoretical results for the interpolation error $\min_{q \in Q_h^1} \|p^* - q_h\|_{L^2}$, cf. Section 2.2 and (4.3). The velocity error in the H^1-norm shows the same $\mathscr{O}(h^{1/2})$ behaviour, whereas in the L^2-norm the error behaves like $\mathscr{O}(h^{3/2})$.

4.1.2. Interface at $\Gamma = \Gamma_2$

We now consider the case $\Gamma = \Gamma_2$. This problem corresponds to the 2D problem discussed in Section 2.2, cf. Fig. 2. Γ is chosen such that $\Gamma \cap F \neq F$ for all faces of the triangulations $\mathscr{T}_0, \mathscr{T}_1, \mathscr{T}_2, \mathscr{T}_3$. As a consequence,

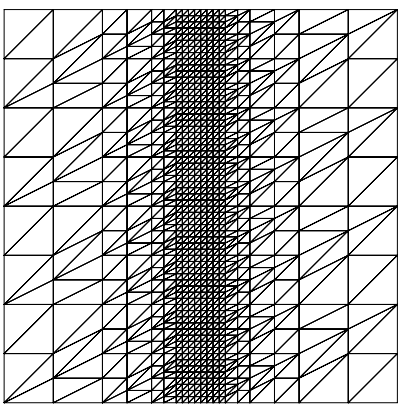

Fig. 6. Slice of grid $\mathscr{T}_h'$ at $x = 0$ after three refinements for $\Gamma = \Gamma_1$.

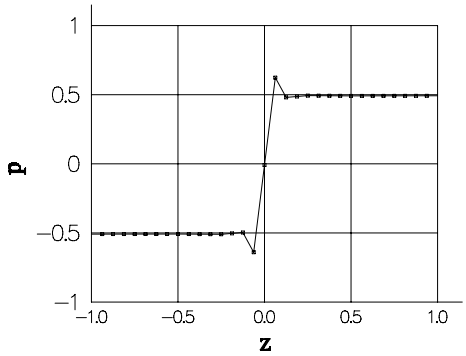

Fig. 7. 1D-profile of pressure jump at $x = y = 0$ for $p_h \in Q_h^1$. Three refinements, $\Gamma = \Gamma_1$.

Table 2
Errors and numerical order of convergence for the $P_2 - Q_h^1$ finite element pair, $\Gamma = \Gamma_1$

# Ref.	$\|e_{\mathbf{u}}\|_{L^2}$	Order	$\|e_{\mathbf{u}}\|_1$	Order	$\|e_p\|_{L^2}$	Order
0	4.26E−02	–	4.26E−01	–	5.32E−01	–
1	1.85E−02	1.2	3.41E−01	0.32	3.78E−01	0.49
2	7.09E−03	1.38	2.55E−01	0.42	2.68E−01	0.5
3	2.60E−03	1.45	1.85E−01	0.46	1.90E−01	0.5
4	9.37E−04	1.47	1.33E−01	0.48	1.34E−01	0.5

$p^* \notin Q_h^0$ and $p^* \notin Q_h^1$, but $p^* \in Q_h^{\Gamma_h}$. We checked that the finite element solution $(\mathbf{u}_h, p_h) \in \mathbf{V}_h \times Q_h^{\Gamma_h}$ is in fact equal to $(\mathbf{u}^*, p^*)$.

Let us first discuss the results for P_1 finite elements. The grid $\mathscr{T}_3$ after 3 times refinement and the corresponding pressure solution for P_1 finite elements are shown in Figs. 8 and 9 respectively. The error norms for different grid refinement levels are shown in Table 3. The same convergence orders as for the case $\Gamma = \Gamma_1$ are obtained, cf. Table 2.

The results for the P_0 finite elements are shown in Table 4. Compared to P_1 finite elements, the errors are slightly larger but show similar convergence orders, i.e. $\mathcal{O}(h^{1/2})$ for the pressure L^2-error and velocity H^1-error as well as $\mathcal{O}(h^{3/2})$ for the L^2 velocity error.

4.2. Test case B: static bubble

We consider test case B for two different approximations of the CSF term f_Γ, namely the "naive" Laplace–Beltrami discretization f_{Γ_h} as in (2.14) and the modified Laplace–Beltrami discretization $\tilde{f}_{\Gamma_h}$ as in (2.17). For

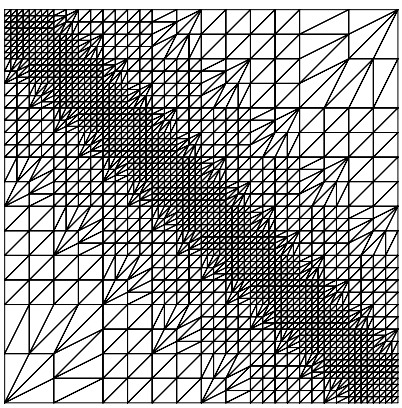

Fig. 8. Slice of grid at $x = 0$ after three refinements for $\Gamma = \Gamma_2$.

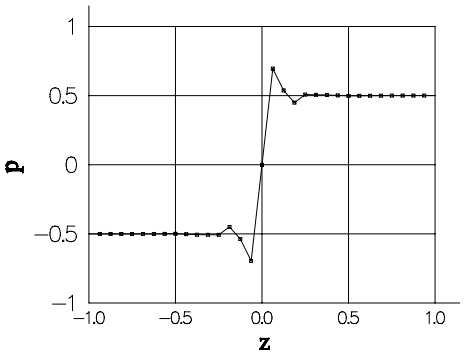

Fig. 9. 1D-profile of pressure jump at $x = y = 0$ for $p_h \in Q_h^1$. Three refinements, $\Gamma = \Gamma_2$.

Table 3
Errors and numerical order of convergence for the $P_2 - Q_h^1$ finite element pair, $\Gamma = \Gamma_2$

# Ref.	$\|e_{\mathbf{u}}\|_{L^2}$	Order	$\|e_{\mathbf{u}}\|_1$	Order	$\|e_p\|_{L^2}$	Order
0	2.53E−02	–	2.56E−01	–	5.44E−01	–
1	1.24E−02	1.02	2.25E−01	0.18	3.99E−01	0.45
2	5.03E−03	1.31	1.75E−01	0.36	2.88E−01	0.47
3	1.89E−03	1.41	1.29E−01	0.44	2.06E−01	0.48
4	6.88E−04	1.46	9.35E−02	0.47	1.46E−01	0.49

Table 4
Errors and numerical order of convergence for the $P_2 - Q_h^0$ finite element pair, $\Gamma = \Gamma_2$

# Ref.	$\|e_{\mathbf{u}}\|_{L^2}$	Order	$\|e_{\mathbf{u}}\|_1$	Order	$\|e_p\|_{L^2}$	Order
0	3.98E−02	–	3.49E−01	–	7.30E−01	–
1	1.64E−02	1.28	2.75E−01	0.35	4.89E−01	0.58
2	6.14E−03	1.41	2.04E−01	0.43	3.35E−01	0.54
3	2.22E−03	1.47	1.48E−01	0.46	2.34E−01	0.52
4	7.92E−04	1.49	1.06E−01	0.48	1.65E−01	0.51

the pressure space we choose $Q_h = Q_h^1$ and $Q_h = Q_h^{\Gamma_h}$. We did not consider the space Q_h^0 as it yields results comparable to those for Q_h^1. Table 5 shows the decay of the pressure L^2-norm for the four different experiments. We observe poor $\mathcal{O}(h^{1/2})$ convergence in the cases where $p_h \in Q_h^1$ or when the surface tension force f_Γ is discretized by f_{Γ_h}. For the L^2 and H^1-norm of the velocity error we observe convergence orders of $\mathcal{O}(h^{3/2})$ and $\mathcal{O}(h^{1/2})$, respectively, which is similar to the results in test case A.

We emphasize that only for the *combination* of the extended pressure finite element space $Q_h^{\Gamma_h}$ with the improved approximation $\tilde{f}_{\Gamma_h}$ we achieve $\mathcal{O}(h^\alpha)$ convergence with $\alpha \geqslant 1$ for the pressure L^2-error. The velocity error in the H^1-norm shows a similar behaviour (at least first order convergence), in the L^2-norm we even have second order convergence, cf. Table 6.

Table 5
Pressure errors for the $P_2 - Q_h^1$ and $P_2 - Q_h^\Gamma$ finite element pair and different discretizations of f_Γ

# Ref.	$\|e_p\|_{L^2}$ for $p_h \in Q_h^1$				$\|e_p\|_{L^2}$ for $p_h \in Q_h^{\Gamma_h}$			
	f_{Γ_h}	Order	$\tilde{f}_{\Gamma_h}$	Order	f_{Γ_h}	Order	$\tilde{f}_{\Gamma_h}$	Order
0	1.60E+00	–	1.60E+00	–	3.12E−01	–	1.64E−01	–
1	1.07E+00	0.57	1.07E+00	0.57	1.00E−01	1.64	4.97E−02	1.73
2	8.23E−01	0.38	8.23E−01	0.38	6.24E−02	0.68	1.66E−02	1.58
3	5.80E−01	0.51	5.80E−01	0.51	4.28E−02	0.54	7.16E−03	1.22
4	4.13E−01	0.49	4.13E−01	0.49	2.95E−02	0.54	2.83E−03	1.34

Table 6
Errors and numerical order of convergence for the $P_2 - Q_h^\Gamma$ finite element pair and improved Laplace–Beltrami discretization $\tilde{f}_{\Gamma_h}$

# Ref.	$\|e_{\mathbf{u}}\|_{L^2}$	Order	$\|e_{\mathbf{u}}\|_1$	Order
0	7.16E−03	–	1.10E−01	–
1	1.57E−03	2.19	4.26E−02	1.37
2	3.25E−04	2.28	1.70E−02	1.33
3	8.57E−05	1.92	7.43E−03	1.19
4	1.75E−05	2.29	2.40E−03	1.63

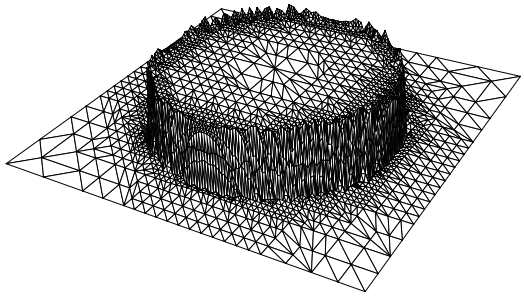

Fig. 10. Finite element pressure solution $p_h \in Q_h^1$ on slice of $\mathscr{T}_4'$ at $z = 0$.

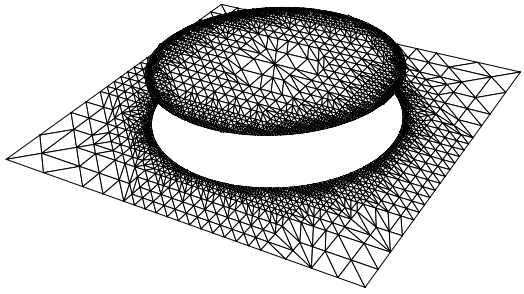

Fig. 11. Finite element pressure solution $p_h \in Q_h^{\Gamma_h}$ on slice of $\mathscr{T}_4'$ at $z = 0$.

For the improved Laplace–Beltrami discretization $\tilde{f}_{\Gamma_h}$ the corresponding pressure solutions $p_h \in Q_h^1$ and $p_h \in Q_h^{\Gamma_h}$ are shown in Figs. 10 and 11, respectively.

4.2.1. μ-dependence of the errors

We repeated the computations of $(\mathbf{u}_h, p_h) \in \mathbf{V}_h \times Q_h^{\Gamma_h}$ for the improved Laplace–Beltrami discretization $\tilde{f}_{\Gamma_h}$ on the fixed grid $\mathscr{T}_3$ varying the viscosity μ. The errors are given in Table 7. We clearly observe that the velocity errors are proportional to μ^{-1} whereas the pressure error is independent of μ. This confirms the bound in (2.10).

Table 7
Errors for the $P_2 - Q_h^\Gamma$ finite element pair and improved Laplace–Beltrami discretization $\tilde{f}_{\Gamma_h}$ on $\mathscr{T}_3$ for different viscosities μ

μ	$\|e_{\mathbf{u}}\|_{L^2}$	$\|e_{\mathbf{u}}\|_1$	$\|e_p\|_{L^2}$
10	8.62E−06	7.51E−04	8.71E−03
1	8.57E−05	7.43E−03	7.16E−03
0.1	8.58E−04	7.44E−02	6.87E−03
0.01	8.57E−03	7.44E−01	6.88E−03
0.001	8.57E−02	7.43E+00	7.16E−03

Remark 4.2. For small μ values the discretization can be improved by adding a grad–div stabilization term to the Stokes equations. In Ref. [28], it is shown that with this term the velocity errors (in $\|\cdot\|_1$) are proportional to $\mu^{-1/2}$ (instead of μ^{-1}) and that for small μ values the discretization errors for the velocity are significantly smaller than without this grad–div term.

5. Outlook

The results for the Stokes test cases presented in Section 4 are quite satisfactory, in the application of the XFEM method to two-phase flow problems, however, there are some hidden pitfalls. We mention two challenges related to stability issues and to the application of XFEM to instationary Navier–Stokes two-phase flow problems.

Regarding stability, one has to treat carefully the situation where the ratio $\frac{|\mathrm{supp}\, q_j^{\Gamma_h}|}{|\mathrm{supp}\, q_j|} \in (0,1)$ for some extended basis function $q_j^{\Gamma_h}$ is either close to zero or close to one, because then the basis functions $q_j, q_j^{\Gamma_h}$ are almost linearly dependent and the resulting system matrices are ill-conditioned. As a consequence, the convergence rate of the iterative solvers can decrease significantly or solvers may even break down. One obvious possibility to deal with this stability problem is to skip the extended basis functions with relatively "small" contributions. A topic of current research is a suitable strategy on how to decide which extended basis functions should be skipped to obtain a (more) stable basis of the extended pressure finite element space which at the same time maintains the desired $\mathcal{O}(h)$ discretization error behaviour. Such a stabilization strategy will be presented in a forthcoming paper.

As $Q_h^{\Gamma_h}$ depends on the location of the interface Γ the space $Q_h^{\Gamma_h}$ changes if the interface is moved. Thus the discretization of $b(\cdot,\cdot)$ has to be updated each time when the level set function (or VOF indicator function) has changed. In a Navier–Stokes code solving instationary two-phase flow problems this is nothing special since mass and stiffness matrices containing discontinuous material properties like density and viscosity have to be updated as well. What is special about the extended pressure finite element space is the fact that the dimension of $Q_h^{\Gamma_h}$ may vary, i.e., some extended pressure unknowns may appear or disappear when the interface is moving. This has to be taken into account by a suitable interpolation procedure for the extended pressure unknowns.

Acknowledgment

This work was supported by the German Research Foundation DFG via the collaborative research center SFB 540.

References

[1] S. Groß, A. Reusken, Finite element discretization error analysis of a surface tension force in two-phase incompressible flows, Preprint 262, IGPM, RWTH Aachen, SIAM J. Numer. Anal. (accepted for publication).
[2] N. Moes, J. Dolbow, T. Belytschko, A finite element method for crack growth without remeshing, Int. J. Numer. Meth. Eng. 46 (1999) 131–150.
[3] T. Belytschko, N. Moes, S. Usui, C. Parimi, Arbitrary discontinuities in finite elements, Int. J. Numer. Meth. Eng. 50 (2001) 993–1013.
[4] S. Pijl, A. Segal, C. Vuik, P. Wesseling, A mass-conserving level-set method for modelling of multi-phase flows, Int. J. Numer. Meth. Fluids 47 (2005) 339–361.
[5] S.B. Pillapakkam, P. Singh, A level-set method for computing solutions to viscoelastic two-phase flow, J. Comp. Phys. 174 (2001) 552–578.
[6] M. Sussman, P. Smereka, S. Osher, A level set approach for computing solutions to incompressible two-phase flow, J. Comp. Phys. 114 (1994) 146–159.
[7] M. Sussman, A.S. Almgren, J.B. Bell, P. Colella, L.H. Howell, M.L. Welcome, An adaptive level set approach for incompressible two-phase flows, J. Comp. Phys. 148 (1999) 81–124.
[8] Y.C. Chang, T.Y. Hou, B. Merriman, S. Osher, A level set formulation of Eulerian interface capturing methods for incompressible fluid flows, J. Comp. Phys. 124 (1996) 449–464.
[9] S. Osher, R.P. Fedkiw, Level set methods: An overview and some recent results, J. Comp. Phys. 169 (2001) 463–502.
[10] J.A. Sethian, Level Set Methods and Fast Marching Methods, Cambridge University Press, Cambridge, 1999.

[11] J.U. Brackbill, D.B. Kothe, C. Zemach, A continuum method for modeling surface tension, J. Comp. Phys. 100 (1992) 335–354.
[12] S. Ganesan, L. Tobiska, Finite element simulation of a droplet impinging a horizontal surface, in: Proceedings of ALGORITMY 2005, 2005, pp. 1–11.
[13] A.-K. Tornberg, Interface Tracking Methods With Application to Multiphase Flows, Phd thesis, Royal Institute of Technology, Department of Numerical Analysis and Computing Science, Stockholm, 2000.
[14] A.-K. Tornberg, B. Engquist, A finite element based level-set method for multiphase flow applications, Comp. Vis. Sci. 3 (2000) 93–101.
[15] X. Yang, A.J. James, J. Lowengrub, X. Zheng, V. Cristini, An adaptive coupled level-set/volume-of-fluid interface capturing method for unstructured triangular grids, J. Comp. Phys. 217 (2006) 364–394.
[16] X. Zheng, A. Anderson, J. Lowengrub, V. Cristini, Adaptive unstructured volume remeshing II: Application to two- and three-dimensional level-set simulations of multiphase flow, J. Comp. Phys. 208 (2005) 191–220.
[17] V. Girault, P.A. Raviart, Finite Element Methods for Navier–Stokes Equations, Springer, Berlin, 1986.
[18] S. Groß, V. Reichelt, A. Reusken, A finite element based level set method for two-phase incompressible flows, Comp. Visual. Sci. 9 (2006) 239–257.
[19] E. Bänsch, Finite element discretization of the Navier–Stokes equations with a free capillary surface, Numer. Math. 88 (2001) 203–235.
[20] S. Ganesan, G. Matthies, L. Tobiska, On spurious velocities in incompressible flow problems with interfaces, Comp. Meth. Appl. Mech. Engng. 196 (2007) 1193–1202.
[21] S. Hysing, A new implicit surface tension implementation for interfacial flows, Int. J. Numer. Meth. Fluids. 51 (2006) 659–672.
[22] J. Chessa, T. Belytschko, An extended finite element method for two-phase fluids, ASME J. Appl. Mech. 70 (2003) 10–17.
[23] A. Hansbo, P. Hansbo, An unfitted finite element method, based on Nitsche's method, for elliptic interface problems, Comp. Meth. Appl. Mech. Engng. 191 (2002) 5537–5552.
[24] P. Hansbo, C. Lovadina, I. Perugia, G. Sangalli, A Lagrange multiplier method for the finite element solution of elliptic interface problems using non-matching meshes, Numer. Math. 100 (1) (2005) 91–115.
[25] J. Mosler, G. Meschke, 3D FE analysis of cracks by means of the strong discontinuity approach, in: Proceedings of European Congress on Comp. Meth. Appl. Sci. Eng. (ECCOMAS), Barcelona, 2000.
[26] S. Groß, A. Reusken, Parallel multilevel tetrahedral grid refinement, SIAM J. Sci. Comput. 26 (4) (2005) 1261–1288.
[27] A. Smolianski, Numerical Modeling of Two-fluid Interfacial Flows, Phd thesis, University of Jyvaskyla, 2001.
[28] M.A. Olshanskii, A. Reusken, Grad–div stabilization for Stokes equations, Math. Comp. 73 (2004) 1699–1718.